Microfluid Nanofluid (2015) 18:559–568
DOI 10.1007/s10404-014-1466-z

RESEARCH PAPER

Plastic light coupler for absorbance detection in silicon microfluidic channels

Heidi Ottevaere · Sara Van Overmeire · Jorge Albero · Lukasz Nieradko · Gert Desmet · Christophe Gorecki · Hugo Thienpont

Received: 30 January 2014 / Accepted: 30 July 2014 / Published online: 8 August 2014

Abstract We present a micro-optical system for ultraviolet/visible absorbance detection in silicon microfluidic channels, which consists of a micro-optical light coupler placed on top of the silicon fluidic channel to probe the molecules under test with laser light. We use nonsequential optical ray-tracing simulations to model the system and to optimize its performance with respect to optical efficiency and system complexity. Deep Proton Writing is used to prototype the plastic light coupler and its spacer baseplate which contains marks to align the micro-optics with respect to the microfluidic channel and which allows for an accurate control of the position of the micro-optics with respect to the excitation source. We demonstrate the proof of concept of this microfluidic light probe by measuring standard samples of coumarin 102 dye with concentrations between 0.6 μM and 6 mM. Calibrating the system yields a detection limit of 4.3 μM. To conclude, we show that the concept of this microfluidic detection system is generic in that it can be applied at different positions on different microfluidic channel configurations.

Keywords Absorbance detection · Microfluidics · Rapid prototyping · Micro-optics

H. Ottevaere (✉) · S. Van Overmeire · H. Thienpont
Brussels Photonics Team B-PHOT, Department of Applied Physics and Photonics, Vrije Universiteit Brussel, Pleinlaan 2, 1050 Brussels, Belgium
e-mail: Heidi.Ottevaere@vub.ac.be

J. Albero · L. Nieradko · C. Gorecki
Département MN2S, UFR ST, FEMTO-ST (UMR CNRS 6174), 16 Route de Gray, 25030 Besançon Cedex, France

G. Desmet
Department of Chemical Engineering, Vrije Universiteit Brussel, Pleinlaan 2, 1050 Brussels, Belgium

1 Introduction

Microfluidic channels ranging from tens to hundreds of micrometer exploit their small size and characteristic laminar microfluidic flow to enable the manipulation and processing of small, nanoliter amounts of fluids. By building complex microfluidic devices, different chemical processes (sample preparation, injection, reaction, separation and detection) can be integrated on a single device (Pang et al. 2012). Such labs-on-chips can offer a fast response time and high performance, low sample consumption, enhanced reliability and sensitivity through process automation, parallelism on a single substrate, portability, disposability and opportunities for low-cost mass production. Portability allows analyses to be carried out outside the laboratory, thereby minimizing the risk of sample contamination and degradation, and offering a faster response at a lower cost. Microfluidic systems will contribute to the development of real-time and on-site testing for biochemical analysis in various application areas such as point-of-care diagnosis, environmental monitoring, biodefense, forensics, food quality control and industrial analysis.

In the past decades, the development of practical microfluidic systems for biochemical analysis has evolved rapidly. However, their applications have been limited to laboratory prototypes without widespread routine use in clinical or high-throughput applications (Mark et al. 2010). This is partly due to technological limitations in two parts of the sample analysis cycle: sample preparation and detection. In particular, detection has since the beginning been one of the main challenges in microfluidics. Indeed, very sensitive techniques must be employed to detect the limited amount of molecules available in the nanoliter detection volumes. Optical detection is one of the

techniques capable of providing sufficient sensitivity but is commonly still accomplished by bulky and expensive microscopes located off-chip. Miniaturized and integrated optical detection systems are therefore needed to fully exploit the potential advantages of microfluidic devices.

In this paper, we focus on optical detection for silicon microfluidic devices. The matured etching and lithographic techniques originally developed in the semiconductor industry to process silicon wafers with nanometer accuracy were a driving force for the development of the first microfluidic circuits. However, the initial silicon chips were gradually replaced by polymeric devices, which can be mass produced by means of simple and cost-effective replication techniques such as injection molding or hot embossing (Becker and Gärtner 2008). Nevertheless, today silicon still remains the material of choice for certain applications because it has several unique properties: simple generation of an inert surface (SiO_2) by oxidation, high-temperature stability, high chemical resistance to organic solvents and acids, well-established bonding and coating processes, an extensive knowledge about coatings, and its well-defined and excellent mechanical properties as a single crystal material. Channel walls are usually very smooth, complex structures can be fabricated, and electric functions such as heaters and sensors can be integrated when required as part of the microfluidic component (Monat et al. 2007).

A key detection technique in conventional biochemical analysis techniques such as electrophoresis and liquid chromatography is ultraviolet (UV)/visible (VIS) absorbance detection, and hence, there is a need to microminiaturize and to implement this technique as well in silicon labs-on-chips. Absorbance detection requires the propagation of an UV or VIS light beam through the microfluidic channel such that the amount of absorbed light can be quantified. Since silicon absorbs UV and VIS light, this is often done by using optical fibers to bring light to the channel and to collect nonabsorbed light (Chandrasekaran and Packirisamy 2008). In this case, the fibers are aligned using microstructured positioning grooves. Other recently reported UV/VIS absorbance detection systems for silicon microfluidic channels use optical waveguides instead of fibers, more in particular silica-on-silicon waveguides fabricated by chemical vapor deposition or flame hydrolysis deposition, and spin-coated polymer waveguides. Silica-on-silicon offers deposition of high-quality, mechanically stable glass films with low optical absorption in the near-UV to near-infrared wavelength range. The refractive index of the deposited glass films can easily be adjusted over a large range (1.45–2.0) simply by changing the composition of the source gasses (Gustafsson et al. 2008). However, the relatively complex, lengthy and costly fabrication processes limit the waveguide thickness to a few micrometers which makes the coupling procedures complicated and may not meet the demand for applications in deeper channels. Therefore, when larger waveguides are required, the employment of less expensive polymer materials with similar optical properties that can be easily deposited and patterned to the required thickness is often preferred (Malic and Kirk 2007). These fiber and waveguide-based techniques are in-plane configurations which deliver and collect the probing light in the wafer plane.

In this paper, we present a different approach for absorbance measurements in silicon microfluidic channels, namely an out-of-plane technique where the probing light enters and exits the sample perpendicularly to the plane of the chip. Such out-of-plane configurations have already been proposed for absorbance detection (Van Overmeire et al. 2008; Verpoorte et al. 1992; Tiggelaar et al. 2002; Salimi-Moosavi et al. 2000), but in this work, we have also miniaturized the optics needed to couple light in and out the detection cell and we have integrated fibers to connect the optics to the source and the detector. As such a compact micro-optical detection unit is created. The schematic of the system is shown in Fig. 1a. We place a polymer micro-optical light coupler on which a metallic coating is deposited on top of the silicon wafer to couple light in and out the fluidic channel. As will be further explained in the next paragraphs, in the practical setup, this coupler will be placed in a polymer spacer baseplate which is not shown in the basic schematic in Fig. 1.

The excitation light is guided through the channel by means of reflections on the metallic-coated surfaces of the coupler and on the oblique sidewalls of the silicon channel. The excitation source and the detector for quantifying the amount of nonabsorbed excitation light can be placed off-chip and can be connected to the chip by optical fibers. Decoupling the optical part from the microfluidics eliminates the need of propagating a UV or VIS light beam in the silicon wafer plane. This way we open up the possibility of reusing the same optics for different microfluidic chips and of combining several couplers to probe a microfluidic channel simultaneously at different locations (Fig. 1b). Since the detection approach is independent of the microfluidic channel configuration, we can build a generic detection system for parallel measurements on different types of microfluidic wafers. Finally, also the fabrication of the optics and the microfluidics can be decoupled and the coupler can be mass produced in plastic by replication methods such as injection molding or hot embossing. Using a light coupler on top of a silicon microfluidic wafer for UV/VIS absorbance measurements is therefore a flexible and cost-effective solution. We remark that this detection configuration is limited to silicon microfluidic wafers bonded to glass plates (as opposed to all-silicon devices) which contain microfluidic channels with oblique sidewalls at the required detection points.

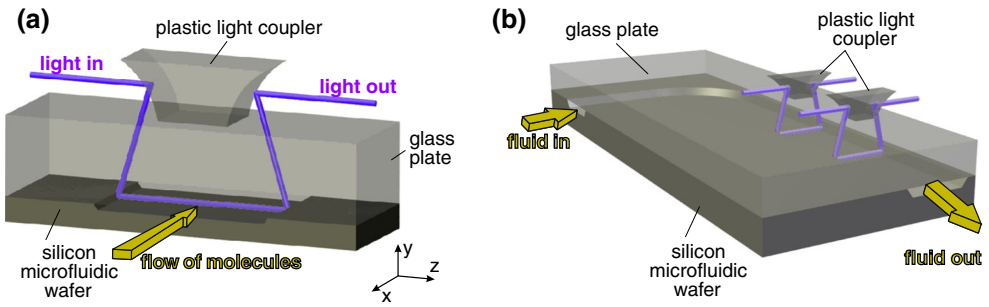

Fig. 1 **a** Schematic of a single detection unit. **b** Illustrating parallelism by probing at different sites on a microfluidic chip

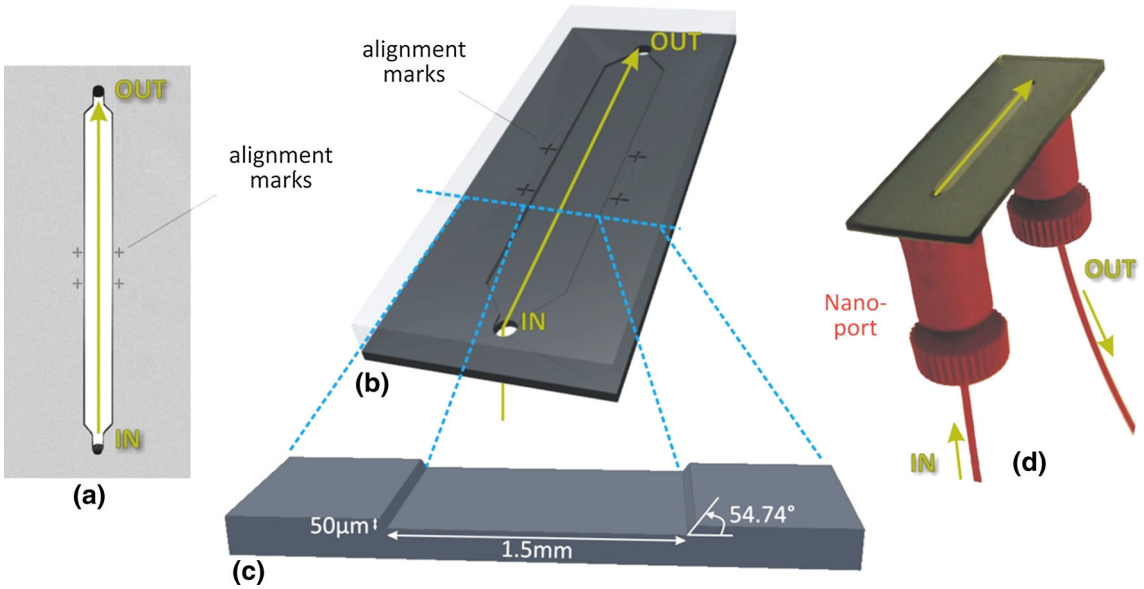

Fig. 2 Microfluidic channel fabricated in silicon by wet anisotropic etching with fluidic in and outlet: **a** *top view* picture of the fabricated channel, **b** schematic, **c** close-up of the cross section of the channel to illustrate the trapezoidal shape of the microchannel and **d** the fabricated microfluidic channel with connections to an external microfluidic circuit

2 Materials and methods

2.1 The microfluidic chip

The optical configuration requires a microfluidic channel with oblique reflecting sidewalls at the probing location. We have constructed a trapezoidal-shaped channel (Fig. 2a–c), using wet anisotropic etching in a silicon wafer (Ziaie et al. 2007). The channel sidewalls have a slope of 54.74° as determined by the anisotropic etching process in silicon. It has a channel width of 1.5 mm to provide a sufficiently large optical path length for absorbance detection. To limit the total detection volume, the channel height is only 50 µm. These cross-sectional dimensions are chosen arbitrarily to construct this first proof-of-concept prototype, but can be changed to suit other applications. Also more complex microfluidic circuits or z-cells with oblique sidewalls could be used. Four alignment marks are patterned around the channel. These will be used for aligning the micro-optics with respect to the chip. A standard Pyrex 7740 glass plate with a thickness of 700 µm is fixed to the silicon chip by anodic bonding. Holes with a diameter of 500 µm, drilled through the bottom of the silicon chip, serve as an in and outlet on which Nanoports (Upchurch Scientific) are glued to provide a leakage-free connection between the channel, the external fluidic pumping system and the waste reservoir (Fig. 2d).

2.2 Optical design

We use nonsequential optical ray-tracing simulations (ASAP^{TM}, Breault Research Organization, Inc.) to model the system and to optimize its performance with respect to optical efficiency and system complexity in terms of the number and the type of optical components used. Nonsequential ray tracing is needed to investigate the propagation

of partially reflected rays and to monitor stray light in the detection unit since in a first stage, no antireflection coatings are considered to limit the cost of the final system. The geometry of the channel as defined in the previous paragraph and the polymer micro-optical components (coupler and baseplate)—the properties of which are to be optimized—is defined in the ray-tracing software. The material of the micro-optical components is defined as poly(methyl methacrylate) (PMMA), as this the material for which the Deep Proton Writing (DPW) technology that will be used to prototype the micro-optics is optimized. For indices of refraction of the different materials (PMMA, glass, silicon) at the working wavelength of 405 nm, the following values are used: $n_{\mathrm{PMMA}} = 1.52$, $n_{\mathrm{glass}} = 1.47$ and $n_{\mathrm{silicon}} = 5.43 + i \times 0.33$. We assume that the channel is completely and uniformly filled with a substance comparable to water with an index of refraction of 1.33. The PMMA coupler sidewalls are surrounded by a uniform 500-nm-thick aluminum layer, to represent the aluminum coating that will be deposited. The source is modeled as the light emerging from a standard single mode fiber (SMF) (SMF28, Corning), as will be used in the final setup to bring light from a laser source to the microfluidic device. The fiber output is represented as the superposition of Gaussian beams. These Gaussian beams can be traced through the optical system by geometric ray-tracing methods implemented in the software. The use of Gaussian beams instead of conventional rays enables a more realistic simulation of the propagation of light emitted by the fiber. The detector surface is modeled as a perfectly absorbing circular surface with a diameter of 600 μm, which is equal to the diameter of the multi mode fiber (MMF) that we will use in the practical setup to guide light to the photodetector (BFH48-600 MMF, Thorlabs). The efficiency of the system is defined as the integrated light energy distribution at the MMF input surface divided by the integrated light energy distribution of the source. We will optimize the parameters of the plastic light coupler to increase the efficiency such that a maximum of light propagates through the channel and reaches the detector.

2.3 Prototyping of micro-optics

For the fabrication of the micro-optical components, we use DPW, a technology to rapidly prototype micro-optical systems that can combine micromechanical positioning structures and refractive micro-optical components (Van Erps et al. 2011). The DPW process is a high-aspect ratio lithographic process in which a micrometer-sized proton beam is used to irradiate an optical grade PMMA sample according to a predefined pattern by translating the sample perpendicularly to the proton beam. The XY translation stages that move the sample in the beam have a positioning accuracy of 50 nm. The irradiated zones can be developed by means of a selective etching solvent, resulting in high-aspect ratio structures with sidewalls featuring optical quality. Typical RMS surface roughness is below 30 nm. As such (2-D arrays of) microholes, cylindrical microlenses and optically flat micromirrors, as well as alignment features and mechanical support structures can be prototyped. Although DPW is not a mass fabrication technique as such, master components prototyped by DPW can be mass produced at low cost with replication techniques such as micro injection molding and hot embossing in a variety of high-tech plastics (Van Erps et al. 2008).

Physical vapor deposition (PVD) using filament-resistive heating (Oerlikon Balzers coating system) was applied to deposit the aluminum coating on the PMMA micro-optical coupler. Typical thicknesses of the deposited layers are between 500 and 700 nm.

2.4 Experimental proof-of-concept demonstration setup

The fabricated microsystem is tested in a proof-of-concept demonstration setup. Excitation light generated by a violet laser diode (iPulse, $\lambda = 405$ nm, 10 mW, Toptica) is on/off modulated at 521 Hz and guided to the microsystem by a SMF (SMF28, Corning). The nonabsorbed excitation light which has propagated through the microfluidic channel is coupled in a large core MMF (BFH48-600, Thorlabs). The light guided through the fiber is spectrally filtered with a band-pass filter (D405/10, AHF Analysentechnik) to select only the excitation wavelength and to suppress possible fluorescence and environmental stray light. The filtered light is quantified by a silicon photodiode (818-UV, Newport). The analog photodiode voltage signal is filtered by two notch filters which remove noise at the line frequency (50 Hz) and twice the line frequency to clean up the detector signal. Afterward, the signal is fed to a lock-in amplifier (SR830, Stanford Research Systems) which extracts and quantifies the signal modulated at the same frequency as the excitation source. To allow efficient lock-in amplification, the modulation frequency should be chosen in a region where there is not too much noise present. In this setup, we observe a large noise component in the detector output around 1 kHz, which is not present at lower frequencies. Therefore, the source is modulated at a lower frequency, here 521 Hz. The settings of the noise filter in the lock-in amplifier can be adjusted to optimize the filtering of noise at frequencies very close to the reference frequency. Large filter time constants, corresponding to small filter bandwidths, provide efficient filtering. However, they cause slow detector response and output smoothing. For this setup, a trade-off was found experimentally for a filter with a time constant of 10 ms and 18 dB roll-off.

The lock-in amplifier voltage output is sampled at 10 Hz, which is the highest sample rate possible in the current hardware configuration. In a practical application, the sample rate should be chosen in function of the smallest sample peaks that need to be analyzed, such that 25 data points per peak can be measured (Perrin et al. 2004). In this proof-of-concept demonstration, we work with the highest sample rate available to enable measurements of various kinds of peaks. If lower sample rates are desired, data bunching, the averaging of a defined number of data points, can be applied to realize the desired frequency. The amplified signal is read out through a GPIB connection by a computer using LabVIEW software and is further processed by means of MATLAB.

The chemical samples under test are delivered to the microfluidic channel by a syringe pump (KD Scientific) connected to a high-pressure switching valve (Rheodyne) with a sample loop of 5 µl. PEEK tubing (Upchurch Scientific) is used to connect the valve to one of the Nanoports glued on the silicon microfluidic chip. The other Nanoport is connected to a waste reservoir.

2.5 Chemicals

To determine experimentally the concentration measurement range and the detection limit, the response of the system on a set of standard samples with known concentration is measured. All samples are prepared from a stock solution consisting of 12 mM coumarin 102 dye (Acros Organics) dissolved in methanol (Sigma Aldrich). As 12 mM is experimentally observed to be the solubility limit for coumarin in methanol, no samples with higher concentrations are studied in this work. Samples at lower concentrations are prepared by dilution of the stock solution with methanol.

From absorbance measurements in a cuvette by means of an optical spectrum analyzer, we derived that the extinction coefficient of coumarin 102 is $1.6 \times 10^4\ \mathrm{M}^{-1}\ \mathrm{cm}^{-1}$ at 405 nm and $2.3 \times 10^4\ \mathrm{M}^{-1}\ \mathrm{cm}^{-1}$ at 385 nm which is the absorption maximum. These values agree very well with the values reported in literature (Brackmann 2000).

2.6 Data processing and analysis

First, the voltage signal I is converted to an absorbance signal A in absorbance units (AU), by using the relation

$$A = -\log\left(\frac{I}{I_0}\right) \tag{1}$$

where I_0 is the average baseline signal measured over 50 data points before the sample is injected such that no absorbing molecules are present in the channel. This absorbance signal is filtered in the time domain by a Savitsky–Golay filter (Felinger 1998) with an order of 3 and a window of 51 points to remove the signal noise. The linear background drift caused by the source, detector and possible solvent variations is fitted with a first-order curve and removed from the absorbance signal (trend-removal). From this resulting absorbance signal, the areas of the measured sample peaks are quantified. To determine the peak boundaries, the first derivative of the signal, representing the slope or the tangent in each point of the signal, is calculated. When the slope exceeds a predefined slope threshold, a peak start is detected. The peak stop is detected where the slope becomes larger than a predefined negative slope threshold. The peak area between the peak start and stop is calculated by trapezoidal numerical integration. Finally, also the signal-to-noise ratio (SNR) is calculated by dividing the peak height by the background noise, where the peak height is defined as the difference between the mean sample signal (calculated from 30 data points at the top of the peak) and the mean background signal (calculated from 30 data points of the baseline preceding the peak) and where the background noise is defined as the standard deviation of the background signal.

3 Results and discussion

3.1 Optical design

The plastic light coupler placed on top of the silicon wafer should provide an efficient and uniform excitation of the molecules in the microfluidic channel. The challenge is to couple the excitation light into the channel, to propagate the light beam over a length of 1.5 mm in the shallow channel with a height of only 50 µm and to couple the nonabsorbed excitation light out of the channel to a detector. In Fig. 3, the complete setup with a ray trace plot is shown. Each light ray emerging from the fiber tip represents a small individual Gaussian beam with a distinct light intensity (highest intensity for beams in the center and lower intensity toward the edges) such that all beams together make up the total output light distribution of the SMF. The divergent beam emerging from the fiber tip should be focused into the channel. To achieve this without adding any extra lenses, the left sidewall of the plastic light coupler is curved. Similarly, the right sidewall of the coupler is curved such that the light beam which is coupled out of the channel can be focused into a MMF which guides the light toward an external detector.

In order to efficiently reflect light in and out the channel, the sidewalls of the plastic light coupler are coated with aluminum. A metallic coating was chosen because its reflection shows a lower angular sensitivity than dielectric

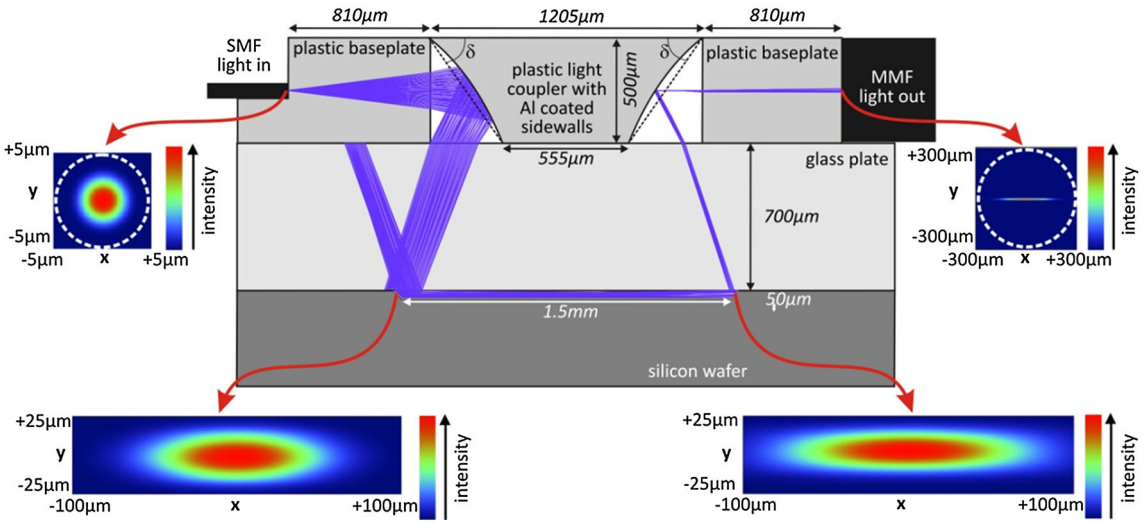

Fig. 3 Schematic of the detection system with an overlaid ray trace and the light distributions at the SMF output, the channel sidewalls and the MMF input

coatings. Both aluminum and silver offer a high reflectivity for visible and more specifically violet wavelengths, e.g., 405 nm as will be used in the actual proof-of-concept demonstration setup. For this application, we choose aluminum to limit the cost of the total system. If the same detection principle would be needed for applications using other wavelengths, another metal might be more appropriate. The material for the coupler, however, can stay PMMA, since the light does not need to propagate through the PMMA material. Remark that in the current design, the sidewalls of the coupler are only curved in the *YZ* plane, as illustrated by the elliptical light energy distributions at the channel sidewalls and the MMF input surface. To collect the complete elliptical light beam coming from the coupler, we use a MMF with a large core of 600 µm.

A spacer baseplate with a fiber groove to position and align the fiber passively with respect to the light coupler is implemented in the simulations. As explained in the next section, this baseplate will also contain marks to assist in the alignment of the micro-optics on the chip. A critical thickness $d_{\text{baseplate}}$ is needed for mechanical strength. Here, a value of 1000 µm was implemented.

The radius of curvature R of the coupler sidewalls and the tilt of the coupler sidewalls (angle δ in Fig. 3) are optimized. We consider a symmetric coupler with equal R and δ for both sidewalls. The highest overall optical efficiency found is 12 % for $R = 1200$ µm and $\delta = 57°$. We observe that in this most optimal configuration, the focus lies at the end of channel and most losses occur at the first channel sidewall. A transmittance of 12 % is of course a relatively low value. However, systems with even lower transmittances (1 %) have been successfully used for absorbance measurements (Mogensen et al. 2003). This indicates that the design presented in this paper should be applicable as well, which will be demonstrated in the next sections.

From the ray tracing in Fig. 3, we can calculate the detection volume: the volume in which molecules are excited and from which nonabsorbed light can be collected. Here, the detection volume equals 15 nl, determined by the optical path length of 1.5 mm and the cross-sectional width of the beam propagating through the channel (200 µm × 50 µm).

In the configuration discussed above, spherical reflecting sidewalls are implemented. No significant improvements were observed when aspheric mirrors are used instead.

3.2 Prototyping of the micro-optics and assembly of the complete microsystem

By means of DPW, we have prototyped the coupler according to the design discussed in the previous paragraph as well as the baseplate which contains a hole to insert the coupler, a fiber groove to insert the fiber and four alignment marks (Fig. 4). As such we can use a combination of active and passive alignment for the alignment of the complete system which is done as follows. The silicon microfluidic chip is aligned actively with the baseplate of the coupler by means of alignment marks on corresponding positions on both components. It is important that the baseplate is parallel and in contact with the silicon chip. Therefore, we fix the baseplate in a clamp which is mounted on an *XYZ* stage, such that it is parallel to the silicon surface. Using the *X* and *Y* adjustment, the baseplate is moved to align the marks on both components. The positions of the marks are visualized using a lens system

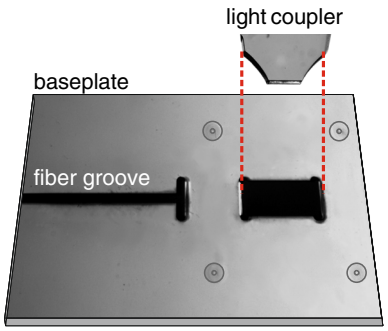

Fig. 4 Microscope picture of the coupler and its baseplate prototyped by DPW. The four sets of concentric circles patterned around the hole for the coupler in the baseplate are the alignment marks corresponding to the marks on the silicon microfluidic chip

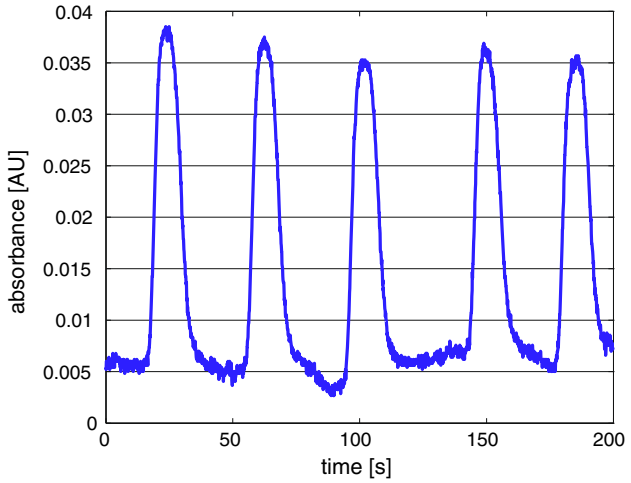

Fig. 5 Absorbance measurement of five consecutive injections of a coumarin 102 sample with a concentration of 60 μM

offering a high magnification at a long working distance (Volpi AG). Using the Z adjustment, the baseplate is slowly lowered, while the alignment of the marks is continuously checked and optimized, until it touches the microfluidic chip. The baseplate could be glued in place by means of, e.g., UV curing glue; however, for this proof-of-concept demonstration, we prefer to keep the possibility of realigning the system. Therefore, no glue is applied. The fibers and the coupler are subsequently placed in grooves etched in the baseplate such that the source and the micro-optics are automatically aligned with the channel and no further active alignment is needed. In a practical setup, the fibers can be glued in place as well, such that a mechanical robust system is created.

In the practical setup, an efficiency of 1 % is reached, which is lower than the simulated efficiency of 12 % (see previous paragraph). Losses could be due to nonideal metallic coatings causing less reflectivity than simulated, scattering of the excitation light and residual misalignments, in particular of the coupler which is the most critical part in the setup. Simulations show that an angular misalignment of the coupler with respect to the baseplate of 0.3° can cause unwanted reflections of the excitation beam such that the efficiency of the system is decreased with 50 %. Despite this low efficiency in the practical setup, sufficient light was coupled in and out the fluidic channel to enable absorbance measurements. As long as light is captured onto the detector and a calibration curve can be set up, a quantitative analysis of concentrations can be performed as will be demonstrated in the next paragraph.

In the future, we will try to adapt the baseplate such that the coupler is not simply inserted in a hole, but is fixed in place using mechanical clip systems or U-shaped alignment features which fit in corresponding holes in the baseplate such that once the coupler is positioned in place, no rotations are possible. This will make the system more robust and increase its stability and efficiency.

3.3 Calibration

Our goal is to use this detection system for quantitative analysis of the concentration of analytical samples. As we do not measure concentration directly, we set up a calibration curve, which provides a mathematical relation between the output of the system (peak area of the absorbance signal) and the sample concentration. As a case study in this paper, we set up a calibration curve for the dye coumarin 102. Five standard solutions with concentrations between 0.6 μM and 6 mM are characterized (see example in Fig. 5). For every concentration, six consecutive injections are measured and the average peak area (in AU s) is calculated (Table 1). Because the six samples have been taken from the same batch, we can assume that the variation on the concentration is negligible for a certain concentration. For the measured peak area, the uncertainties have been calculated using the standard deviation (SD) and the relative standard deviation (%RSD) of the peak area (Moore 2010). We observe that the precision, represented by the standard deviation, obtained for the replicated measurements is not constant for all concentrations (heteroscedasticity), which is commonly observed when large concentration ranges are considered (Vander Heyden et al. 2007). Therefore, we will apply weighted least squares regression techniques on the data points to obtain the mathematical representation of the calibration curve.

The theoretical Lambert–Beer model predicts a linear relation between the absorbance signal and sample concentration (Parson 2009):

$$A = \varepsilon \cdot C \cdot l \tag{2}$$

where ε is the extinction or molar absorption coefficient, C the sample concentration and l the optical path length. However, in practical applications, nonlinear relations have

Table 1 Average peak area measurements (in AU s) with SD, %RSD and average SNR (for each concentration average of six measurements)

Concentration (M)	Peak area (Au s)	SD (Au s)	%RSD	SNR
6×10^{-3}	1.9283×10^{-1}	3.7×10^{-3}	2.0	20321
6×10^{-4}	2.4513×10^{-2}	7.4×10^{-4}	3.0	3099
6×10^{-5}	2.44×10^{-3}	1.2×10^{-4}	5.1	268
6×10^{-6}	2.89×10^{-4}	2.2×10^{-5}	7.5	61
6×10^{-7}	6.2×10^{-5}	2.1×10^{-5}	34	14

been observed (Wätzig 1995). A major cause for nonlinearity is stray light which can reach the detector without passing through the detection cell such that the detector will report an incorrectly low absorbance (Wiese et al. 1990; Petersen et al. 2002). This effect is more pronounced at higher concentrations because the stray light becomes a larger fraction of the total transmitted light. The resulting calibration curve is first linear and saturates at high concentrations such that the maximum measurable absorbance level is limited. Between the linear range and saturation, there is a region where the curve is deviating from linearity but which is still usable to predict the concentration from a measured absorbance signal. In addition to stray light, other mechanisms can cause deviations from the linear Lambert–Beer relation such as detector noise and dark currents when only a low amount of light reaches the detector. To take into account possible nonlinearities in our system, we verify both linear and nonlinear regression techniques. The quality of the fit is given by the correlation coefficient R^2, which gives the correlation between the response values and the predicted response values and which should be as close as possible to 1, and by the sum of squares due to error (SSE), which measures the total deviation of the response values from the fit to the response values and which should be as small as possible. Adding parameters to the model increases R^2 and decreases SSE, however, at the risk of overfitting the data, which is reflected in a large confidence interval and a large standard error on the estimated value of the parameters.

We first consider all measured data points such that the complete concentration range from 0.6 µM to 6 mM is taken into account. A linear relation ($y = a \cdot x + b$) and a power fit ($y = a \cdot x^b$) are applied. The linear relationship $y = a \cdot x + b$ results in an intercept b which is less than one standard error SE_b away from zero ($b < SE_b$). This can be considered as normal variation, allowing to force the curve through zero ($b = 0$, $y = a \cdot x$) (Boqué and Vander 2009). A quadratic polynomial fit ($y = a \cdot x^2 + b \cdot x + c$) was also tried but is not usable, as the standard errors of the resulting parameters are very large (>100 %), which suggests overfitting. The estimated parameters and the goodness-of-fit statistics for the different curve fits are shown in Table 2. The power model gives the best goodness-of-fit parameters, indicating that there is some nonlinearity present, most probably due to stray light caused by excitation light reaching the detector without propagating through the channel due to small angular misalignment of the coupler with respect to the baseplate and by the non-ideal reflecting metallic coatings.

To investigate if only the highest measured concentration causes nonlinearity, in a next step, we reduce the upper limit of the considered concentration range from 6 mM to 0.6 mM and apply again least squares regression. As $b > SE_b$, the linear curve cannot be forced through zero. For this reduced concentration range, the linear model gives the best results (Table 2).

From the calibration curve, we can calculate the limit of detection (LOD), which is defined as the lowest concentration of a component that will lead, with a probability of $(1 - \beta)$, to the conclusion that this measured concentration is larger than that of a blank sample (Boqué and Vander 2009). A value of 0.05 for β is recommended by the International Union of Pure and Applied Chemistry (1998). Although the detection system will sometimes detect smaller concentrations than the LOD, the LOD represents the smallest concentration that can be detected in a reliable way. For peak area calibration, several procedures for LOD estimation have been suggested (Boqué and Vander 2009; Dolan 2009). Here, we apply the method suggested by Boqué et al. The injection and measurement of each sample was replicated six times for statistical analysis. For a sample with a concentration close to the expected LOD, the measured detector responses are converted to concentrations using the calibration curve. The standard deviation of these concentrations σ_C is used to calculate the LOD (Boqué and Vander 2009):

$$LOD = 3.3 \cdot \sigma_C \tag{3}$$

As shown in Table 2, an LOD of 4.3 µM is found using the linear calibration obtained for the concentration range from 0.6 µM to 0.6 mM. Other authors use as guideline for peak area calibration that the LOD should be measurable with a relative standard deviation (%RSD) of ≈17 % (Dolan 2009), which is confirmed by the results in Table 1, where the detection limit should lie between 6 µM (%RSD = 7.5) and 0.6 µM (%RSD = 34). Finally, the LOD can also be determined as the lowest concentration for which the measured absorbance signal has an SNR of at least 3.3 (Currie 1999). Using this approach, we can conclude from Table 1 that the LOD is 0.6 µM. This SNR-based LOD is lower than the one obtained using peak area calibration, as the SNR takes into account the peak height instead of area. In general, peak height measurements are

Table 2 Goodness-of-fit statistics for peak area calibration with a and b the fitting coefficients, SSE the sum of squares due to error, R^2 the correlation coefficient and LOD the limit of detection

Concentration range	Fitting equation	a	b	SSE	R^2	LOD (10^{-6} M)
6×10^{-7} M–6×10^{-3} M	$y = a \cdot x$	34.3 ± 3.5	/	48	0.9885	5.1
	$y = a \cdot x^b$	23.7 ± 3.8	0.937 ± 0.023	11	0.9974	3.7
6×10^{-7} M–6×10^{-4} M	$y = a \cdot x + b$	40.62 ± 0.70	$(4.1 \pm 1.0) \times 10^{-5}$	0.2	0.9999	4.3
	$y = a \cdot x^b$	33 ± 14	0.973 ± 0.050	4	0.9971	3.9

not susceptible to integration errors. As such they are more precise and suitable to quantify small peaks in trace analysis and to analyze partly overlapping peaks. However, in general peak area, measurements give more accurate results under peak broadening conditions, as the peak area remains proportional to the total quantity of substance passing into the detector (Guiochon and Guillemin 1988). Therefore, here 4.3 μM is considered as the LOD of the system. The LOD could be further improved by reducing the amount of stray light in the system. This can be achieved by improving the shielding of the setup from environmental stray light and by improving the alignment of the coupler in the baseplate such that all excitation light is coupled into the microfluidic channel. One could also try to increase the sensitivity of the system by increasing the optical path length. However, for a longer optical path length, the coupling of light into the channel with a height of only 50 μm height will be more complicated. As such only a small amount of light will propagate through the system and the baseline noise will be increased (Felinger 1998). Therefore, a trade-off should be targeted between the path length and the amount of transmitted power to find the optimum sensitivity in terms of the SNR. In deeper channels, coupling losses will be reduced, however, at the expense of increased peak broadening in the detector due to the increased detection volume.

For a correct comparison of the detection, performance with other state-of-the-art systems, not only the LOD but also the detection volume and the optical path length available in the system, and the type of molecule tested and in particular its molar absorptivity should be taken into account. Remark that for systems featuring a similar optical path length, it is important to consider the cross section of the detection cell and as such the total detection volume as well, because in large detection cells, it is easier to couple light in and out such that a lower LOD can be obtained. The out-of-plane approach by Tiggelaar et al. yielded a very low LOD of 0.002 μM for indophenol blue ($\varepsilon = 2 \times 10^4$ M^{-1} cm^{-1}), however, in a system with a large detection volume of 720 nl featuring an optical path length of 6 mm (Tiggelaar et al. 2002). In waveguide-based UV–VIS absorbance detection systems, smaller detection volumes and optical path lengths are used. An LOD of 15 μM was reported for Bromothymol blue dye detection ($\varepsilon = 2.65 \times 10^4$ M^{-1} cm^{-1}) in a system with a detection volume of 2 nl and an optical path length of 1 mm (Mogensen et al. 2003). An LOD of 1 μM was obtained for Alexafluor dye detection ($\varepsilon = 10^5$ M^{-1} cm^{-1}) in a detection volume of 1 nl and an optical path length of 500 μM (Malic and Kirk 2007). With our system, which has a detection volume of 12 nl and an optical path length of 1.5 mm and which was tested with a dye having a molar absorptivity of 1.6×10^4 M^{-1} cm^{-1}, an LOD in the same order of magnitude as the waveguide-based systems was obtained. The advantage of this system, however, is its out-of-plane architecture which allows the construction of a versatile, generic detection system that can measure at different positions on one microfluidic wafer or that can be easily reconfigured for different microfluidic channel configurations.

4 Conclusion

We have presented a novel cost-effective approach for UV/VIS absorbance measurements in silicon microfluidic channels, implementing a micro-optical light coupler on top of the silicon wafer to couple light in and out the fluidic channel, instead of propagating a UV or visible light beam in the plane of the silicon wafer by using embedded optical fibers or waveguides. Decoupling the optics from the microfluidics opens opportunities in terms of low-cost mass production of the optics and the development of generic detection systems for parallel measurements on different types of microfluidic circuits. The detection system was designed using optical ray-tracing simulations, prototyped in PMMA by means of DPW and applied on a trapezoidal-shaped microfluidic test channel fabricated in silicon by means of wet etching. The performance of the system was studied in a proof-of-concept demonstration setup. Coumarin dye samples with molar concentrations from 0.6 μM to 6 mM were characterized. Using peak area calibration, an LOD of 4.3 μM was found. This is comparable to the performance reached with state-of-the-art miniaturized waveguide-based detection systems.

In the future, we will investigate the efficiency of asymmetric light couplers featuring different curvatures at their input and output surfaces as well as the use of couplers with sidewalls that are curved both in the XZ and the YZ plane

such that the light is focused in all directions, as opposed to the elliptical light beam in the current configuration, which will enable the excitation of smaller plugs of molecules inside the channel. We will also integrate a fluorescence collection light path in the system such that both absorbance and fluorescence measurements can be used for characterization of molecules in the microfluidic channel. Fluorescence is more sensitive and will offer lower LODs, however, at the cost of labeling nonfluorescent molecules.

Finally, this detection approach is not limited to silicon microfluidic channels only, but could also be applied in glass or polymer microfluidic chips. The possibility of this material change is important because of the trend of gradually replacing silicon chips by polymeric devices, which can be mass produced by means of simple and cost-effective replication techniques such as injection molding or hot embossing. In a polymer-based microfluidic chip, the channel sidewalls in the detection region will also be oblique but coated with a metallic mirror and covered with a transparent top plate to allow the propagation of the light reflected by the coupler into the channel. As such we can conclude that the presented technique is not only limited to chips containing silicon baseplates, but it is a much more versatile optical probing technique that can be applied in a variety of microfluidic channels for multiple applications without compromising the LOD.

Acknowledgments This work was supported in part by DWTC-IAP, FWO, GOA, the 6th FP European Network of Excellence on Micro-Optics NEMO, the 7th FP European Network of Excellence on Biophotonics Photonics 4 Life, the Methusalem and Hercules foundations and the OZR of the Vrije Universiteit Brussel (VUB). The authors would like to thank M. Vervaeke and J. Van Erps of the Brussels Photonics Team (VUB-B-PHOT) and the members of the Department of Chemical Engineering (VUB-CHIS).

References

Becker H, Gärtner C (2008) Polymer microfabrication technologies for microfluidic systems. Anal Bioanal Chem 390:89–111

Boqué R, Vander HeydenY (2009) The limit of detection. LC–GC Eur 22:82–85

Brackmann U (2000) Lambdachrome laser dyes, 3rd edn. Lambda Physik AG, Goettingen

Chandrasekaran A, Packirisamy M (2008) Integrated optical microfluidic lab-on-a-chip. In: Proceedings of SPIE 7099 70992B-1-8

Currie LA (1999) Detection and quantification limits: origins and historical overview. Anal Chim Acta 391:127–134

Dolan JW (2009) Calibration curves part 2: what are the limits? LC–GC Eur 22:244–247

Felinger A (1998) Data analysis and signal processing in chromatography. Elsevier Science B.V., Amsterdam

Guiochon G, Guillemin CL (1988) Quantitative gas chromatography: for laboratory analyses and on-line process control. Elsevier Science B.V., Amsterdam

Gustafsson O, Mogensen KB, Ohlsson PD, Liu Y, Jacobson SC, Kutter JP (2008) An electrochromatography chip with integrated waveguides for UV absorbance detection. J Micromech Microeng 18:055021

International Union of Pure and Applied Chemistry (IUPAC) (1998) Presentation of the results of chemical analysis. In: Inczedy J, Lengyel T, Ure AM, Gelencser A, Hulanicki A (eds) Compendium of analytical nomenclature, 3rd edn, chap 2. Blackwell, Oxford

Malic L, Kirk AG (2007) Integrated miniaturized optical detection platform for fluorescence and absorption spectroscopy. Sens Actuators A 135:515–524

Mark D, Haeberle S, Roth G, von Stetten F, Zengerle R (2010) Microfluidic lab-on-a-chip platforms: requirements, characteristics and applications. Chem Soc Rev 39:1153–1182. doi:10.1039/B820557B

Mogensen KB, El-Ali J, Wolff A, Kutter JP (2003) Integration of polymer waveguides for optical detection in microfabricated chemical analysis systems. Appl Opt 42:4072–4079

Monat C, Comachuk R, Eggleton BJ (2007) Integrated optofluidics: a new river of light. Nat Photonics 1:106–114

Moore DS (2010) The basic practice of statistics, Chap 2. W. H. Freeman & Company, New York

Pang L, Fainman Y, Chen HM, Freeman LM (2012) Optofluidic devices and applications in photonics, sensing and imaging. Lab Chip 12:3543–3551

Parson WW (2009) Modern optical spectroscopy student edition. Springer, Berlin

Perrin C, Fabre H, Massart DL, Vander Heyden Y (2004) Electrophoresis 24:2469–2480

Petersen NJ, Mogensen KB, Kutter JP (2002) Performance of an in-plane detection cell with integrated waveguides for UV/Vis absorbance measurements on microfluidic separation devices. Electrophoresis 23:3528–3536

Salimi-Moosavi H, Jiang Y, Lester L, McKinnon G, Harrison DJ (2000) A multireflection cell for enhanced absorbance detection in microchip-based capillary electrophoresis devices. Electrophoresis 21:1291–1299

Tiggelaar RM, Veenstra TT, Sanders RGP, Gardeniers JGE, Elwenspoek MC, van den Berg A (2002) Talanta 56:331–339

Van Erps J, Wissmann M, Guttmann M, Hartmann M, Mohr J, Debaes C, Thienpont H (2008) Hot embossing of microoptical components prototyped by Deep Proton Writing. IEEE Photonics Technol Lett 20:1539–1541

Van Erps J, Vervaeke M, Debaes C, Ottevaere H, Hermanne A, Thienpont H (2011) Rapid prototyping technology—principles and functional requirements. In: Hoque ME(ed) Publ. Intech ISBN 978-953-307-970-7

Van Overmeire S, Ottevaere H, Nieradko L, Marc P, Mappes T, Mohr J, Gorecki C, Thienpont H (2008) Plastic light coupler for absorbance detection in silicon microfluidic devices, MOC'08 conf. proc. 92–93

Vander Heyden Y, Boqué Rodríguez R, Cuesta M (2007) Calibration. LC-GC Europe 20

Verpoorte E, Manz A, Lüdi H, Bruno AE, Maystre F, Krattiger B, Widmer HM, van der Schoot BH, de Rooij NF (1992) A silicon flow cell for optical detection in miniaturized total chemical analysis systems. Sens Actuators B 6:66–70

Wätzig H (1995) Appropriate calibration functions for capillary electrophoresis—I. Precision and sensitivity using peak areas and heights. J Chromatogr A 700:1–7

Wiese A, Teitz K, Brombacher V, Höschele G, Kuderer H (1990) A new generation of LC absorbance detectors. Hewlett–Packard J 41:36–43

Ziaie B, Baldi A, Atashbar M (2007) Introduction to micro/nanofabrication. In: Bhushan B (ed) Handbook of nanotechnology. Springer, Berlin, pp 197–233